Appl Biol Chem (2016) 59(2):217–225
DOI 10.1007/s13765-016-0149-8

Online ISSN 2468-0842
Print ISSN 2468-0834

ARTICLE

Isoflavones as modulators of adenosine monophosphate-activated protein kinase

Hyeryoung Jung[1] · Seunghyun Ahn[1] · Beum Soo Kim[1] · Soon Young Shin[2] · Young Han Lee[2] · Yoongho Lim[1]

Received: 2 November 2015 / Accepted: 9 November 2015 / Published online: 29 January 2016

Abstract Adenosine monophosphate-activated protein kinase (AMPK) is expressed in all eukaryotic cells and can therefore be found in vertebrates, invertebrates, and plants. Since AMPK participates in the regulation of homeostasis on various levels, small compounds that can modulate AMPK activity could be valuable research tools. Several flavonoids can modulate AMPK. Here we investigated the modulatory effect of 37 isoflavones on AMPK activity using an in vitro kinase assay. Because the relationship between the structural properties of flavonoids and their modulatory activities has not been elucidated yet, we used comparative molecular field analysis to derive the structural conditions for modulation of AMPK activity. The molecular binding mode of isoflavones to AMPK was elucidated using in silico docking studies. The findings presented here can aid in the design of new modulators with better specificity for AMPK.

Keywords Adenosine monophosphate-activated protein kinase · Isoflavone · Quantitative structure-activity relationship · In silico docking · Kinase

H. Jung and S. Ahn have contributed equally to this work.

Electronic supplementary material The online version of this article (doi:10.1007/s13765-016-0149-8) contains supplementary material, which is available to authorized users.

✉ Yoongho Lim
yoongho@konkuk.ac.kr

[1] Division of Bioscience and Biotechnology, BMIC, Konkuk University, Seoul 143-701, Korea

[2] Department of Biological Sciences, Konkuk University, Seoul 143-701, Korea

Introduction

Adenosine monophosphate (AMP)-activated protein kinase (AMPK) is expressed in all eukaryotic cells and is present in vertebrates, invertebrates, and plants (Ghillebert et al. 2011). It was first identified in 1988, and mammalian AMPK was purified and sequenced in 1994 (Munday et al. 1988; Mitchelhill et al. 1994). Although AMPK was discovered only recently, a large body of knowledge exists on its function because it plays various roles in the regulation of homeostasis. AMPK regulates carbohydrate metabolism, including glycolysis, glycogen metabolism, and glucose uptake, sensing, and production. It is also involved in lipid metabolism, including cholesterol synthesis and fatty acid partitioning and uptake, mitochondrial biogenesis, and protein metabolism, including cell growth and apoptosis (Steinberg and Kemp 2009). AMPK consists of three subunits, α, β, and γ, which are highly conserved across different eukaryotic species (Hardie et al. 2003). Because AMPK has a heterotrimeric structure, 12 heterotrimeric combinations are possible (Hardie et al. 2012). In mammalian cells, two isoforms of the α subunit, two isoforms of the β subunit, and three isoforms of the γ subunit are known (Carling 2004). The α and γ subunits contain a β-binding domain and the β subunit has both α- and γ-binding domains (Goransson et al. 2007). These binding domains are conserved in all α, β, and γ isoforms. The three-dimensional (3D) structures of human AMPK have been determined using X-ray crystallography (Xiao et al. 2013; Li et al. 2015).

Since AMPK participates in the regulation of homeostasis at various levels, several studies have set out to discover small compounds that can control AMPK activity. Berberine, an isoquinoline alkaloid, has been used for the

therapy of type II diabetes in Korea (Choi et al. 2015). and can activate AMPK (Brusq et al. 2006). Metformin is another stimulator of AMPK activity (Musi et al. 2002) that has been used for type II diabetes treatment (Knowler et al. 2002). The fatty acid α-lipoic acid also activates AMPK (Lee et al. 2006) as does resveratrol, a plant-derived polyphenol (Zang et al. 2006). Different flavonoids, including anthocyanin, (−)-epigallocatechin-3-gallate, naringenin, naringin, tangeritin, and fisetin have also been shown to modulate AMPK (Hajiaghaalipour et al. 2015). In a previous study, we demonstrated that apigenin and trihydroxyflavone inhibit AMPK, while kaempferide and trihydroxymethoxyflavone activate AMPK (Yong et al. 2015). Flavonoids are plant-derived polyphenols, all of which shave a C6-C3-C6 skeleton as their common structural feature. Flavonoids with a 4*H*-chromen-4-one C6-C3 structure are referred to as flavones and those with a chroma-4-one structure as flavanones. Among the flavonoids mentioned above, tangeritin and fisetin belong to the flavones, while naringenin and naringin are flavanones. A further distinction can be made between 2-phenyl-4*H*-chromen-4-one and 3-phenyl-4*H*-chromen-4-one compounds, which are classified as flavones and isoflavones, respectively. Genistein, formonetin, prunetin, and daidzein belong to the category of isoflavones, and they all modulate AMPK (Ahn et al. 2013; Andersen et al. 2014; Cheong et al. 2014; Sanchez et al. 2008). Although almost 10,000 papers on AMPK can be found on PubMed, only one paper covers the relationships between the structural properties of the compounds that regulate AMPK and their activity (Wang et al. 2011). However, that study did not include flavonoids; thus, virtually nothing is known about the relationship between the structural properties of flavonoids and their effects on AMPK. We investigated isoflavones as modulators of AMPK using an in vitro kinase assay and derived the structural conditions for improved effects on AMPK from quantitative structure–activity relationship (QSAR) calculations. The molecular binding mode of isoflavones to AMPK was elucidated through in silico docking studies.

Materials and methods

We studied 37 isoflavones, which were purchased from Indofine Chemicals (Hilsborough, NJ, USA). They all contained hydroxy or methoxy groups, and 4 isoflavones were also glycosylated. Their structures and names are listed in Table 1. The in vitro kinase assay of AMPK was performed using the Z'-LYTE Kinase Assay kit (Invitrogen, Carsbad, CA, USA) which contains AMPK α1β1γ1. All materials for the kinase assay were used as provided in the kit and other materials were purchased from local suppliers. We followed the procedures provided by the manufacturer's manual and a previously reported method (Yong et al. 2015). The concentrations of AMPK and ATP were adjusted to 0.49 nM and 50 μM, respectively. The phosphorylation of AMPK at Thr172 is required for its activity (Hawley et al. 1996). A peptide, AlaMetAlaArgAlaAlaSerAlaAlaAlaLeuAlaArgArgArg, was used as the AMPK substrate. A 96-well-plate reader (Molecular Devices, Sunnyvale, CA) was used to measure fluorescence resonance energy transfer between coumarin and fluorescein where excitation was given at 400 nm and emission signals for coumarin and for fluorescein were obtained at 445 and 520 nm, respectively. The concentration of the test compounds was 40 μM. The AMPK induction values of the test compounds were determined relative to the AMPK induction obtained at 100 % phosphorylation. All experiments were iterated three times. The relative activity of AMPK in the presence of the tested isoflavones ranged between 62 and 108 %, and is listed in Table 1 for each compound. To obtain the modulatory activity of each isoflavone, the corresponding relative AMPK activity was normalized to that of the condition showing the strongest inhibitory effect. Negative logarithmic scales were used for the QSAR calculations, which are listed in Table 1.

The QSAR calculations were performed using comparative molecular field analysis (CoMFA) on an Intel Core 2 Quad Q6600 (2.4 GHz) Linux PC with the molecular modeling package Sybyl 7.3 (Tripos, St. Louis, MO) (Hyun et al. 2012). To obtain the 3D structures of the tested isoflavones, the X-ray crystallographic structure of 4′-hydroxy-7-methoxyisoflavone deposited in the Protein Data Bank (1FP2.pdb) was used as a template (Zubieta et al. 2001). All test compounds were sketched using the Sybyl program based on the 3D structure of 4′-hydroxy-7-methoxyisoflavone. The most stable structures were determined following previously reported methods (Shin et al. 2014). Likewise, CoMFA was carried out following previously published methods (Shin et al. 2014).

Results and discussion

The results obtained from the in vitro kinase assay were confirmed using Western blot analysis. Preadipocytes 3T3L1 (American Type Culture Collection, Manassas, VA, USA) were cultured in Dulbecco's modified Eagle's medium supplemented with 10 % fetal bovine serum (Hyclone, Logan, UT, USA). Following treatment with 40 μM isoflavones, the 3T3L1 cells were harvested and lysed in 20 mM 4-(2-hydroxyethyl)-1-piperazineethanesulfonic acid buffer (pH 7.2), 1 % Triton X-100, 10 % glycerol, 150 mM NaCl, 10 μg/mL leupeptin, and 1 mM phenylmethylsulfonyl fluoride. Electrophoresis and

Table 1 Structures and names of 37 isoflavone derivatives and their negative logarithmic activity values (pAc)

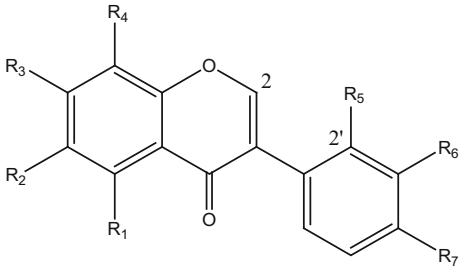

Number	Name	R_1	R_2	R_3	R_4	R_5	R_6	R_7	pAc
1	4′-acetoxy-7-hydroxy-6-methoxyisoflavone	H	OCH_3	OH	H	H	H	$OCOCH_3$	0.801
2	4′-bromo-5,7-dimethoxyisoflavone	OCH_3	H	OCH_3	H	H	H	Br	0.763
3	6-chloro-7-methylisoflavone	H	Cl	CH_3	H	H	H	H	0.780
4	6-chloro-4′,7-dimethoxyisoflavone	H	Cl	OCH_3	H	H	H	OCH_3	0.806
5	4′-chloro-7-methoxy-8-methylisoflavone	H	H	OCH_3	CH_3	H	H	Cl	0.824
6	4′-chloro-5,7-dimethoxyisoflavone	OCH_3	H	OCH_3	H	H	H	Cl	0.838
7	2′-chloro-5,7-dimethoxyisoflavone	OCH_3	H	OCH_3	H	Cl	H	H	0.848
8	4′-chloro-7-hydroxy-8-methylisoflavone	H	H	OH	CH_3	H	H	Cl	0.824
9	4′,7-dihydroxyisoflavone-8-C-glucoside	H	H	OH	Glu	H	H	OH	0.806
10	2′,6-dichloro-7-methoxyisoflavone	H	Cl	OCH_3	H	Cl	H	H	0.801
11	4′,5-dihydroxy-7-metoxyisoflavone	OH	H	OCH_3	H	H	H	OH	0.906
12	4′,7-dihydroxyisoflavone	H	H	OH	H	H	H	OH	0.900
13*	5,7-dihydroxy-4′-methoxyisoflavone	OH	H	OH	H	H	H	OCH_3	0.895
14	5-hydroxy-4′,7-dimethoxyisoflavone	OH	H	OCH_3	H	H	H	OCH_3	0.848
15	7-hydroxy-3′,4′-dimethoxyisoflavone	H	H	OH	H	H	OCH_3	OCH_3	0.824
16	4′,7-dimethoxyisoflavone	H	H	OCH_3	H	H	H	OCH_3	0.810
17*	4′,7-dimethoxy-8-methylisoflavone	H	H	OCH_3	CH_3	H	H	OCH_3	0.775
18	7-hydroxy-4′,6-dimethoxyisoflavone	H	OCH_3	OH	H	H	H	OCH_3	0.806
19	4′-methoxyisoflavone-7-O-glucoside	H	H	OGlu	H	H	H	OCH_3	0.810
20	4′-hydroxyisoflavone-7-O-glucoside	H	H	OGlu	H	H	H	OH	0.829
21*	7-hydroxy-8-methylisoflavone	H	H	OH	CH_3	H	H	H	0.973
22	7-hydroxyisoflavone	H	H	OH	H	H	H	H	0.759
23	4′-hydroxy-6-methoxyisoflavone-7-O-glucoside	H	OCH_3	OGlu	H	H	H	OH	0.788
24*	7-hydroxy-6-mehtoxyisoflavone	H	OCH_3	OH	H	H	H	H	0.824
25	7-methoxyisoflavone	H	H	OCH_3	H	H	H	H	0.759
26	7-methoxy-8-methylisoflavone	H	H	OCH_3	CH_3	H	H	H	0.784
27	7-methoxy-5-methylisoflavone	CH_3	H	OCH_3	H	H	H	H	0.829
28	2′,4′,6-trichloro-7-methylisoflavone	H	Cl	CH_3	H	Cl	H	Cl	0.788
29	3′,4′,7-trihydroxyisoflavone	H	H	OH	H	H	OH	OH	1.000
30	4′,7,8-trihydroxyisoflavone	H	H	OH	OH	H	H	OH	0.947
31	4′,5,7-trimethoxyisoflavone	OCH_3	H	OCH_3	H	H	H	OCH_3	0.843
32	4′,7,8-trimethoxyisoflavone	H	H	OCH_3	OCH_3	H	H	OCH_3	0.819
33	3′,4′,7-trimethoxyisoflavone	H	H	OCH_3	H	H	OCH_3	OCH_3	0.801
34*	4′,6,7-trihydroxyisoflavone	H	OH	OH	H	H	H	OH	0.788
35	4′,6,7-trimethoxyisoflavone	H	OCH_3	OCH_3	H	H	H	OCH_3	0.771
36*	3′,4′,6,7-tetramethoxyisoflavone	H	OCH_3	OCH_3	H	H	OCH_3	OCH_3	0.806
37*	3′,4′,5,7-tetramethoxyisoflavone	OCH_3	H	OCH_3	H	H	OCH_3	OCH_3	0.780

An asterisk (*) denotes a test set used for QSAR calculations. Glu denotes glucose

immunoblotting were performed as previously described (Shin et al. 2013). Anti-phospho-AMPKα (Thr172) was purchased from Cell Signaling Technology (Beverly, MA, USA). Signals were detected using an enhanced chemiluminescence detection system (Amersham Pharmacia Biotech, Inc., Piscataway, NJ, USA) (Yong et al. 2015).

To elucidate the molecular binding between isoflavones and AMPK, in silico docking was analyzed on an Intel Core 2 Quad Q6600 (2.4 GHz) Linux PC with Sybyl 7.3 software, following previously published methods (Yoon et al. 2013). The 3D structures of human AMPK have been determined and deposited in the Protein Data Bank, and the 3D structure with the best resolution was chosen for in silico docking studies.

The lowest AMPK activity was noted upon treatment with the isoflavone derivative 3′,4′,7-trihydroxyisoflavone (62 %, named TIF, **29**), while treatment with 7-hydroxyisoflavone (108 %, named HIF, **22**) and 7-methoxyisoflavone (108 %, named MIF, **25**) resulted in the highest relative AMPK activity (Fig. 1). To validate the results obtained from the QSAR calculations, first, a test set was chosen based on the hierarchical clustering analysis (Pirhadi and Ghasemi 2010). As shown in Supplementary Fig. 1, the seven derivatives (**13**, **17**, **21**, **24**, **34**, **36**, and **37**)

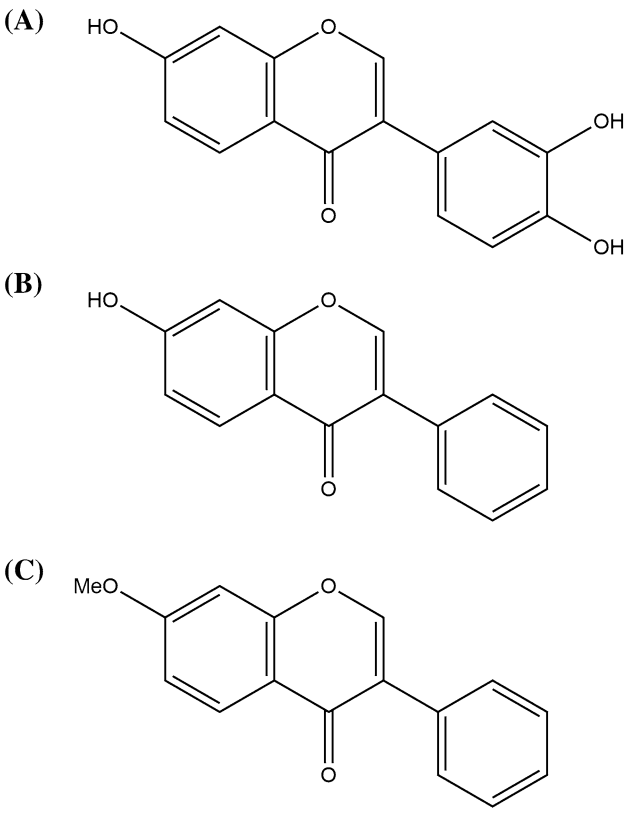

Fig. 1 Structures of (**A**) 3′,4′,7-trihydroxyisoflavone (derivative **29**), (**B**) 7-hydroxyisoflavone (derivative **22**), and (**C**) 7-methoxyisoflavone (derivative **25**)

selected as a test set belong to different structural groups. The training set except the test set was aligned for the identification of interactions between probe atoms and the rest of the molecule using the Sybyl/DATABASE Alignment module. As shown in Supplementary Fig. 2, all derivatives of the training set were aligned and a consistent superposition was obtained. The linear correlation between the calculated fields, including electrostatic and steric fields, and the experimental data was obtained using partial least squares regression. Several CoMFA models were built. To enhance the values of the cross-validation correlation coefficient (q^2) and the non-cross-validated coefficient (r^2), the region-focusing method was applied, with the standard deviation coefficient value ranging from 0.3 to 1.2 and the grid spacing values from 0.5 to 1.5. When q^2, r^2, the standard deviation coefficient, and the grid spacing values were 0.672, 0.974, 0.8, and 1.0, respectively, the best model was selected and the electrostatic and steric field contributions were 41.6 and 58.4 %, respectively. The optimal number of components, the standard error of estimate, and F-values were 6, 0.01, and 141.808, respectively. The experimental data in the training set were compared with the values predicted from the CoMFA model mentioned above and listed in Table 2. The residuals between the experimental data and the predicted values ranged between 0.04 and 2.68 % for the training set. For the test set, which was selected based on the hierarchical clustering analysis, the residuals between the experimental data and predicted values ranged from 4.50 to 20.07 %. Thus, we concluded that our CoMFA model is reliable. The experimental data were plotted against the predicted values (Supplementary Fig. 3). To visualize field contributions obtained from the CoMFA model, contour maps were generated using the Sybyl program. In the case of the steric field, the steric bulky-favored region contributed 20 %, and the disfavored region contributed 80 %. In the contour map for the electrostatic field, the electropositive-group-favored region and the electronegative-group-favored region contributed 93 and 7 %, respectively (Supplementary Fig. 4). Here, 'favor' refers to the activation of AMPK. The bulky substituents at the C-3′ position increase the activation of AMPK. Derivatives **15**, **33**, **36**, and **37** all have methoxy groups at C-3′ and showed lower pAc values than derivative **29**. The electrostatic substituents at C-3′ contribute to the inhibitory effects on AMPK. Derivative **29** has a hydroxy group at C-3′ and showed higher pAc values than derivatives **15**, **33**, **36**, and **37**.

The results from the in vitro AMPK kinase assay showed that 3′,4′,7-trihydroxyisoflavone inhibited AMPK, while 7-hydroxyisoflavone and 7-methoxyisoflavone activated AMPK. To confirm these results, immunoblot analysis was performed using preadipocyte 3T3L1 cells. As

Table 2 Experimental and predicted values with residual values for the training and test sets

Derivative	Activity (pAc)	ω = 0.8/1.0 predicted value	Residual (%)
1	0.801	0.791	−1.24
2	0.763	0.760	−0.39
3	0.780	0.777	−0.39
4	0.806	0.814	0.95
5	0.824	0.821	−0.41
6	0.838	0.849	1.26
7	0.848	0.836	−1.44
8	0.824	0.824	−0.04
9	0.806	0.800	−0.71
10	0.801	0.804	0.34
11	0.906	0.917	1.20
12	0.900	0.888	−1.29
13*	0.895	0.855	−4.50
14	0.848	0.847	−0.14
15	0.824	0.817	−0.80
16	0.810	0.807	−0.34
17*	0.775	0.815	5.19
18	0.806	0.804	−0.29
19	0.810	0.825	1.80
20	0.829	0.817	−1.42
21*	0.973	0.778	−20.07
22	0.759	0.779	2.68
23	0.788	0.794	0.81
24*	0.824	0.768	−6.80
25	0.759	0.773	1.89
26	0.784	0.774	−1.31
27	0.829	0.820	−1.12
28	0.788	0.784	−0.50
29	1.000	1.000	−0.02
30	0.947	0.951	0.38
31	0.843	0.834	−1.04
32	0.819	0.819	0.03
33	0.801	0.808	0.87
34*	0.788	0.909	15.40
35	0.771	0.779	1.04
36*	0.806	0.773	−4.10
37*	0.780	0.832	6.68

The asterisk (*) denotes the test set and ω means the standard deviation coefficient/the grid spacing value used for the region-focusing method

shown in Fig. 2A, serum starvation for 24 h increased the level of AMPK phosphorylation on Thr-172 in the activation loop of the kinase domain, which indicates the activation of AMPK. This increase was substantially reduced by treatment with 10 % fetal bovine serum (FBS). However, when serum-starved cells were treated with 10 % FBS in the presence of 7-hydroxyisoflavone (**22**) or 7-methoxyisoflavone (**25**), the serum-induced decrease in AMPK phosphorylation was prevented, indicating that derivatives **22** and **25** activate AMPK activity (Fig. 2A). On the contrary, when serum-starved cells were treated with sunitinib, a potent AMPK inhibitor (Laderoute et al. 2010), the serum starvation-induced increase of AMPK phosphorylation was attenuated (Fig. 2B). Similarly, treatment with 3′,4′,7-trihydroxyisoflavone (**29**) reduced the serum starvation-induced increase in AMPK phosphorylation. These data demonstrate that isoflavone derivatives **22** and **25** activate AMPK activity, while compound **29** potentially inhibits AMPK activity.

To understand the molecular binding between AMPK and the three derivatives mentioned above, in silico docking studies were carried out using the Sybyl program. Among the different 3D structures deposited in the Protein Data Bank (PDB) are two human AMPK structures (Xiao et al. 2013; Li et al. 2015). Because 4cfe.pdb had a better resolution, we used it for our in silico docking studies. Human AMPK consists of three subunits, α, β, and γ, which are composed of 552, 270, and 331 residues, respectively. The structure deposited as 4cfe.pdb is a hexamer, with two sets of each subunit. Chain A (α2 subunit) contains 519 residues (8–295 and 321–551), chain B (β1 subunit) has 193 residues (78–270), and chain E (γ1 subunit) has 299 residues (27–325) (Xiao et al. 2013). These three chains consist of more residues than chains C (α2 subunit), D (β1 subunit), and F (γ1 subunit), which is why a trimer of A, B, and E chains was chosen for the analysis. To obtain the 3D structure in solution, 4cfe.pdb was subjected to energy minimization. The process was ceased based on the total energy convergence criterion (0.05 kcal/moll Å). The crystallographic structure of 4cfe.pdb contains two ligands, the activator benzimidazole 992 (Supplementary Fig. 5A) and the inhibitor staurosporine (Supplementary Fig. 5B). Therefore, two apoproteins of AMPK were obtained from the energy-minimized structure by the deletion of each ligand using the Sybyl program. The binding site of staurosporine was determined based on the previously reported results of 4cfe.pdb and on the LigPlot analysis (Kramer et al. 1999; Xiao et al. 2013). Because staurosporine resides in chain A (α2 subunit), all residues in the binding site are part of chain A: Leu22, Gly23, Val24, Gly25, Val30, Ala43, Glu94, Val96, Glu100, and Glu143. The radius for the flexible docking was set to 6.5 Å. Before the docking process, the original inhibitor, staurosporine was docked into the apo-AMPK without staurosporine. The ligand was returned to its normal complex. The docking process for derivative **29**, 3′,4′,7-trihydroxyisoflavone, was performed as for staurosporine. Since the docking process was iterated 30 times, 30 different AMPK-ligand complexes were

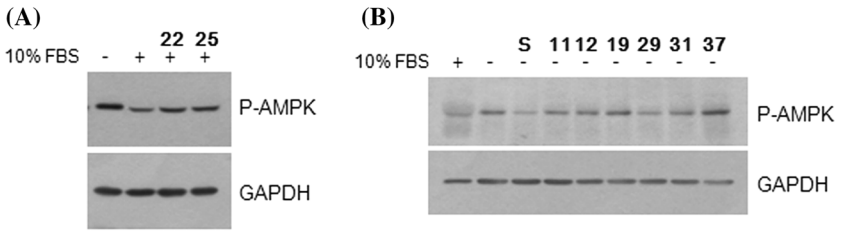

Fig. 2 Effect of isoflavone derivatives on the phosphorylation of AMPK. (**A**) 3T3L1 preadipocytes were starved from serum for 24 h, and subsequently incubated with 10 % FBS in the absence or presence of compound **22** (40 μM) or **25** (40 μM) for 30 min. (**B**) 3T3L1 preadipocytes were starved from serum for 24 h, and subsequently incubated with either 10 % fetal bovine serum or 40 μM derivative compounds. Whole-cell lysates were prepared for immunoblot analysis with anti-phospho AMPK (Thr172). Glyceraldehyde 3-phosphate dehydrogenase (GAPDH) was used as an internal control. *S* denotes the AMPK inhibitor sunitinib

obtained. Their binding energies ranged from -21.18 to -13.76 kcal/mol. Because the first complex had the lowest binding energy and the best docking pose, it was selected for the study of the molecular binding between AMPK and 3′,4′,7-trihydroxyisoflavone. As shown in Fig. 3A, Leu22, Gly23, Val24, Gly25, Val30, Asn144, and Leu146 are involved in the hydrophobic interactions and Val96 formed a hydrogen bond (H-bond). Six residues are found in both the AMPK-3′,4′,7-trihydroxyisoflavone complex and the AMPK-staurosporine complex: Leu22, Gly23, Val24, Gly25, Val30, and Val96. While 3′,4′,7-trihydroxyisoflavone forms one H-bond with AMPK, staurosporine forms four H-bonds with the Glu94, Val96, Glu100, and Glu143 of AMPK. Moreover, while 10 residues are involved in the binding of staurosporine (Fig. 3B), the binding site of 3′,4′,7-trihydroxyisoflavone consists of only nine residues. The binding energy of the AMPK-staurosporine complex ranges from -40.63 to -26.12 kcal/mol and is much lower than that of the AMPK-3′,4′,7-trihydroxyisoflavone complex. Staurosporine can inhibit AMPK at the nanomolar level. In this study, 40 μM of 3′,4′,7-trihydroxyisoflavone inhibits AMPK by only 62 %. Thus, the weaker inhibitory effect of 3′,4′,7-trihydroxyisoflavone can be explained by the weaker molecular binding between AMPK and 3′,4′,7-trihydroxyisoflavone. The 3D images of 3′,4′,7-trihydroxyisoflavone and staurosporine residing in the binding site of AMPK were generated using the PyMol program (The PyMOL Molecular Graphics System, Version 1.0r1, Schrödinger, LLC, Portland, OR) (Figs. 4A, B).

As mentioned above, the crystallographic structure of 4cfe.pdb contains not only an inhibitor, but also an activator, benzimidazole 992. Two derivatives, 7-hydroxyisoflavone (**22**) and 7-methoxyisoflavone (**25**), activated AMPK and their binding modes with AMPK were also studied. First, apo-AMPK, without benzimidazole 992, was prepared in the same manner as for staurosporine. Its binding site was determined based on previously reported results for 4cfe.pdb and on the LigPlot analysis (Xiao et al. 2013). Bound benzimidazole 992 resides in both chain A (α2 subunit) and chain B (β1 subunit), and its binding site consists of Leu18 (A), Val24 (A), Gly28 (A), Lys29 (A), Lys31 (A), Arg83 (B), Arg107 (B), Serine phosphate108 (B), and Asn111 (B) (Supplementary Fig. 6A). From the 30 AMPK-7-hydroxyisoflavone complexes obtained during the flexible docking process, the 23rd complex showed the best docking pose. Therefore, it was selected for the study of the binding mode, even though it did not exhibit the lowest binding energy. The LigPlot analysis indicated that the AMPK-7-hydroxyisoflavone complex includes one hydrophobic interaction with Ile46 (A) and three H-bonds with Lys29 (A), Arg83 (B), and Asn111 (B) (Supplementary Fig. 6B). While nine residues participated in the binding of benzimidazole 992, the binding site of 7-hydroxyisoflavone consisted of four residues. In addition, the binding energy between AMPK and benzimidazole 992 ranged from −22.75 to −17.33 kcal/mol, while that between AMPK and 7-hydroxyisoflavone ranged from −18.43 to −12.46 kcal/mol. These results explain why the AMPK activation by 7-hydroxyisoflavone (108 % at 40 μM) is much weaker than that by benzimidazole 992 (60 nM). Likewise, the docking process was carried out for 7-methoxyisoflavone. The LigPlot analysis showed that the AMPK-7-methoxyisoflavone complex includes one hydrophobic interaction with Ile46 (A) and 3 H-bonds with Lys29 (A), Arg83 (B), and Asn111 (B) (Supplementary Fig. 6C). Its binding energy ranged from -15.89 to -12.77 kcal/mol. As a result, the binding between AMPK on one hand and 7-methoxyisoflavone and 7-hydroxyisoflavone on the other hand, are similar.

Several isoflavones, including genistein, puerarin, sophoricoside, daidzein, and formonetin, have a modulatory effect on AMPK (Andersen et al. 2014; Cheong et al. 2014; Noh et al. 2011; Palacios-Gonzalez et al. 2014; Sanchez et al. 2008; Wu et al. 2013). In our previous report, biochanin A, daidzein, formonetin, and genistein showed inhibitory effects at 100 μM, while glycitein activated AMPK at 100 μM (Yong et al. 2015). The current study evaluated the effect of 37 isoflavones in an in vitro

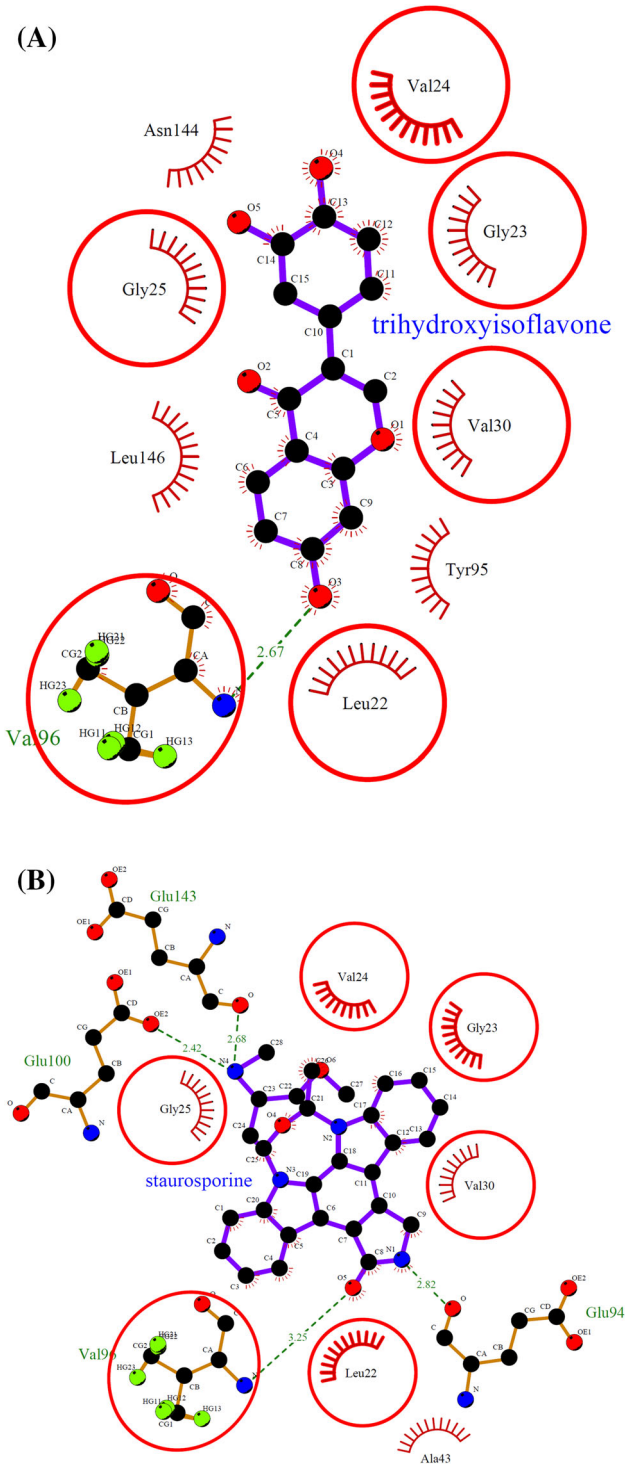

Fig. 3 The binding sites of (**A**) 3′,4′,7-trihydroxyisoflavone and (**B**) staurosporine in AMPK were analyzed by the LigPlot program. *Red arches* indicate the residues participating in hydrophobic interactions and the *dotted lines* indicate hydrogen bonds. Full *red circles* denote the residues present in the binding sites of both 3′,4′,7-trihydroxyisoflavone and staurosporine

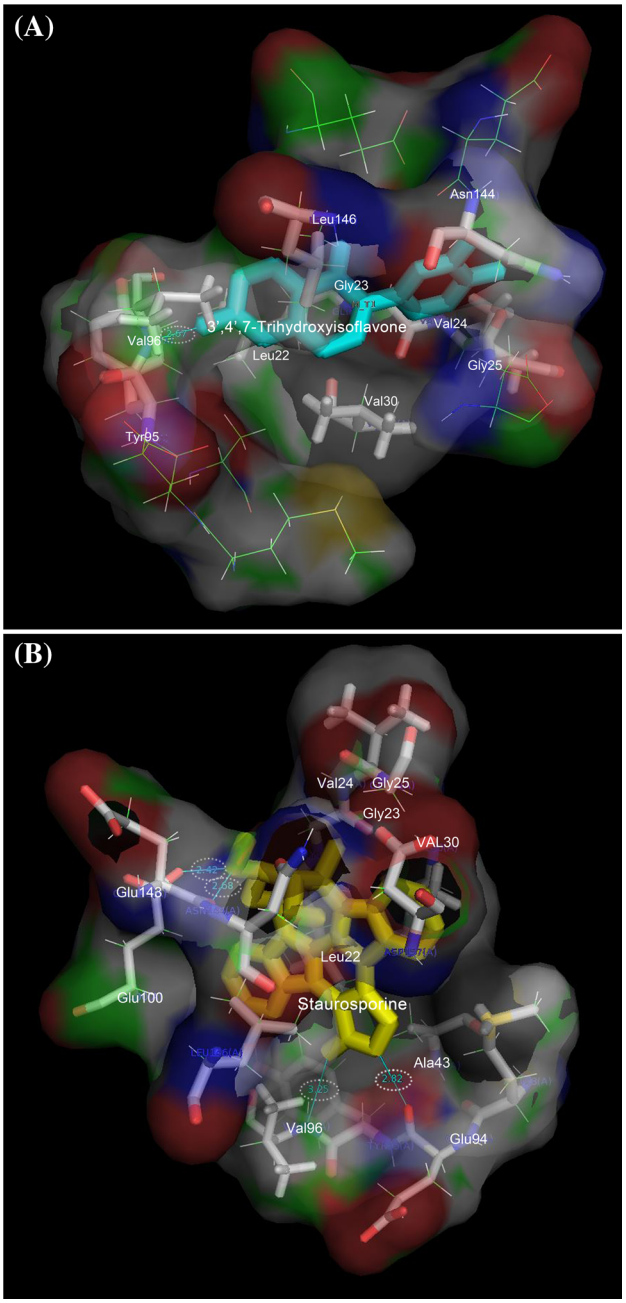

Fig. 4 The 3D image of the binding site of the (**A**) 3′,4′,7-trihydroxyisoflavone-AMPK and (**B**) the staurosporine-AMPK complex, generated using the PyMOL program. 3′,4′,7-trihydroxyisoflavone and staurosporine are colored in *cyan* and *yellow*, respectively

kinase assay and confirms that isoflavones modulate AMPK. Comparative molecular field analysis (CoMFA) demonstrated that bulky or electrostatic substituents at the C-3′ position in isoflavones are important for the modulatory activity towards AMPK. The results obtained in the

in vitro kinase assay were confirmed by Western blot analysis. In addition, the reason why 3′,4′,7-trihydroxyisoflavone shows a weaker inhibitory effect on AMPK than staurosporine was elucidated based on in silico docking studies. In the context of AMPK activation, the binding of 7-hydroxyisoflavone and 7-methoxyisoflavone to AMPK was also compared to that of benzimidazole 992 using in silico docking. These findings can aid in the design of new compounds with improved modulatory activities towards AMPK.

Acknowledgments This paper was supported by Konkuk University in 2013.

References

Ahn TG, Yang G, Lee HM, Kim MD, Choi HY, Park KS, Lee SD, Kook YB, An HJ (2013) Molecular mechanisms underlying the anti-obesity potential of prunetin, an O-methylated isoflavone. Biochem Pharmacol 85:1525–1533

Andersen C, Kotowska D, Tortzen CG, Kristiansen K, Nielsen J, Petersen RK (2014) 2-(2-Bromophenyl)-formononetin and 2-heptyl-formononetin are PPARgamma partial agonists and reduce lipid accumulation in 3T3-L1 adipocytes. Bioorg Med Chem 22:6105–6111

Brusq JM, Ancellin N, Grondin P, Guillard R, Martin S, Saintillan Y, Issandou M (2006) Inhibition of lipid synthesis through activation of AMP kinase: an additional mechanism for the hypolipidemic effects of berberine. J Lipid Res 47:1281–1288

Carling D (2004) The AMP-activated protein kinase cascade—a unifying system for energy control. Trends Biochem Sci 29:18–24

Cheong SH, Furuhashi K, Ito K, Nagaoka M, Yonezawa T, Miura Y, Yagasaki K (2014) Daidzein promotes glucose uptake through glucose transporter 4 translocation to plasma membrane in L6 myocytes and improves glucose homeostasis in Type 2 diabetic model mice. J Nutr Biochem 25:136–143

Choi JS, Ali MY, Jung HA, Oh SH, Choi RJ, Kim EJ (2015) Protein tyrosine phosphatase 1B inhibitory activity of alkaloids from Rhizoma Coptidis and their molecular docking studies. J Ethnopharmacol 171:28–36

Ghillebert R, Swinnen E, Wen J, Vandesteene L, Ramon M, Norga K, Rolland F, Winderickx J (2011) The AMPK/SNF1/SnRK1 fuel gauge and energy regulator: structure, function and regulation. FEBS J 278:3978–3990

Goransson O, McBride A, Hawley SA, Ross FA, Shpiro N, Foretz M, Viollet B, Hardie DG, Sakamoto K (2007) Mechanism of action of A-769662, a valuable tool for activation of AMP-activated protein kinase. J Biol Chem 282:32549–32560

Hajiaghaalipour F, Khalilpourfarshbafi M, Arya A (2015) Modulation of glucose transporter protein by dietary flavonoids in type 2 diabetes mellitus. Int J Biol Sci 11:508–524

Hardie DG, Scott JW, Pan DA, Hudson ER (2003) Management of cellular energy by the AMP-activated protein kinase system. FEBS Lett 546:113–120

Hardie DG, Ross FA, Hawley SA (2012) AMP-activated protein kinase: a target for drugs both ancient and modern. Chem Biol 19:1222–1236

Hawley SA, Davison M, Woods A, Davies SP, Beri RK, Carling D, Hardie DG (1996) Characterization of the AMP-activated protein kinase kinase from rat liver and identification of threonine 172 as the major site at which it phosphorylates AMP-activated protein kinase. J Biol Chem 271:27879–27887

Hyun J, Shin SY, So KM, Lee YH, Lim Y (2012) Isoflavones inhibit the clonogenicity of human colon cancer cells. Bioorg Med Chem Lett 22:2664–2669

Knowler WC, Barrett-Connor E, Fowler SE, Hamman RF, Lachin JM, Walker EA, Nathan DM, Diabetes Prevention Program Research Group (2002) Reduction in the incidence of type 2 diabetes with lifestyle intervention or metformin. N Engl J Med 346:393–403

Kramer B, Rarey M, Lengauer T (1999) Evaluation of the FLEXX incremental construction algorithm for protein-ligand docking. Proteins 37:228–241

Laderoute KR, Calaoagan JM, Madrid PB, Klon AE, Ehrlich PJ (2010) SU11248 (sunitinib) directly inhibits the activity of mammalian 5'-AMP-activated protein kinase (AMPK). Cancer Biol Ther 10:68–76

Lee Y, Naseem RH, Park BH, Garry DJ, Richardson JA, Schaffer JE, Unger RH (2006) Alpha-lipoic acid prevents lipotoxic cardiomyopathy in acyl CoA-synthase transgenic mice. Biochem Biophys Res Commun 344:446–452

Li X, Wang L, Zhou XE, Ke J, de Waal PW, Gu X, Tan MH, Wang D, Wu D, Xu HE, Melcher K (2015) Structural basis of AMPK regulation by adenine nucleotides and glycogen. Cell Res 25:50–66

Mitchelhill KI, Stapleton D, Gao G, House C, Michell B, Katsis F, Witters LA, Kemp BE (1994) Mammalian AMP-activated protein kinase shares structural and functional homology with the catalytic domain of yeast Snf1 protein kinase. J Biol Chem 269:2361–2364

Munday MR, Campbell DG, Carling D, Hardie DG (1988) Identification by amino acid sequencing of three major regulatory phosphorylation sites on rat acetyl-CoA carboxylase. Eur J Biochem 175:331–338

Musi N, Hirshman MF, Nygren J, Svanfeldt M, Bavenholm P, Rooyackers O, Zhou G, Williamson JM, Ljunqvist O, Efendic S, Moller DE, Thorell A, Goodyear LJ (2002) Metformin increases AMP-activated protein kinase activity in skeletal muscle of subjects with type 2 diabetes. Diabetes 51:2074–2081

Noh BK, Lee JK, Jun HJ, Lee JH, Jia Y, Hoang MH, Kim JW, Park KH, Lee SJ (2011) Restoration of autophagy by puerarin in ethanol-treated hepatocytes via the activation of AMP-activated protein kinase. Biochem Biophys Res Commun 414:361–366

Palacios-Gonzalez B, Zarain-Herzberg A, Flores-Galicia I, Noriega LG, Aleman-Escondrillas G, Zarinan T, Ulloa-Aguirre A, Torres N, Tovar AR (2014) Genistein stimulates fatty acid oxidation in a leptin receptor-independent manner through the JAK2-mediated phosphorylation and activation of AMPK in skeletal muscle. Biochim Biophys Acta 1841:132–140

Pirhadi S, Ghasemi JB (2010) 3D-QSAR analysis of human immunodeficiency virus entry-1 inhibitors by CoMFA and CoMSIA. Eur J Med Chem 45:4897–4903

Sanchez Y, Amran D, Fernandez C, de Blas E, Aller P (2008) Genistein selectively potentiates arsenic trioxide-induced apoptosis in human leukemia cells via reactive oxygen species generation and activation of reactive oxygen species-inducible protein kinases (p38-MAPK, AMPK). Int J Cancer 123:1205–1214

Shin SY, Yoon H, Hwang D, Ahn S, Kim DW, Koh D, Lee YH, Lim Y (2013) Benzochalcones bearing pyrazoline moieties show anti-colorectal cancer activities and selective inhibitory effects on aurora kinases. Bioorg Med Chem 21:7018–7024

Shin SY, Jung H, Ahn S, Hwang D, Yoon H, Hyun J, Yong Y, Cho HJ, Koh D, Lee YH, Lim Y (2014) Polyphenols bearing cinnamaldehyde scaffold showing cell growth inhibitory effects

on the cisplatin-resistant A2780/Cis ovarian cancer cells. Bioorg Med Chem 22:1809–1820

Steinberg GR, Kemp BE (2009) AMPK in health and disease. Physiol Rev 89:1025–1078

Wang Z, Huo J, Sun L, Wang Y, Jin H, Yu H, Zhang L, Zhou L (2011) Computer-aided drug design for AMP-activated protein kinase activators. Curr Comput Aided Drug Des 7:214–227

Wu C, Luan H, Wang S, Zhang X, Wang R, Jin L, Guo P, Chen X (2013) Modulation of lipogenesis and glucose consumption in HepG2 cells and C2C12 myotubes by sophoricoside. Molecules 18:15624–15635

Xiao B, Sanders MJ, Carmena D, Bright NJ, Haire LF, Underwood E, Patel BR, Heath RB, Walker PA, Hallen S, Giordanetto F, Martin SR, Carling D, Gamblin SJ (2013) Structural basis of AMPK regulation by small molecule activators. Nat Commun 4:3017–3026

Yong Y, Shin SY, Jung Y, Jung H, Ahn S, Chong Y, Lim Y (2015) Flavonoids activating adenosine monophosphate-activated protein kinase. J Korean Soc Appl Biol Chem 58:13–19

Yoon H, Kim TW, Shin SY, Park MJ, Yong Y, Kim DW, Islam T, Lee YH, Jung KY, Lim Y (2013) Design, synthesis and inhibitory activities of naringenin derivatives on human colon cancer cells. Bioorg Med Chem Lett 23:232–238

Zang M, Xu S, Maitland-Toolan KA, Zuccollo A, Hou X, Jiang B, Wierzbicki M, Verbeuren TJ, Cohen RA (2006) Polyphenols stimulate AMP-activated protein kinase, lower lipids, and inhibit accelerated atherosclerosis in diabetic LDL receptor-deficient mice. Diabetes 55:2180–2191

Zubieta C, He XZ, Dixon RA, Noel JP (2001) Structures of two natural product methyltransferases reveal the basis for substrate specificity in plant O-methyltransferases. Nat Struct Biol 8:271–279